15th IFK
Proc. of the 15th International Fluid Power Conference <Symposium/Conference>
<DOI>

Non-destructive Detection of Fatigue Cracks in Hydraulic Components

Boden, Lukas[1*]; Blatter, Fabian[2]; Marcus Geimer [2], Katharina Schmitz [1]

1. RWTH Aachen University – Institute for Fluid Power Drives and Systems (ifas),
2. Institute of Mobile Machines, Karlsruhe Institute of Technology, Karlsruhe, German

*lukas.boden@ifas.rwth-aachen.de

Abstract.

As hydraulic components continue to evolve toward higher power densities and efficiencies, their structural design must meet increasingly demanding performance and reliability requirements. This often requires a targeted, sustainable use of material, particularly in highly stressed regions. This demands the assessment of the components' load limits, which are determined by cyclic pressure impulse tests.

During operation most components fail due to fatigue cracks, which have severe consequences. Thus, detailed knowledge of crack-growth behaviour is essential. Crack-propagation depends on the material properties and, above all, on the local stress amplitudes at the crack tip. The latter is changed in fluid power applications since the viscous oil interacts with the crack faces. This study aims to investigate the effect on a large scale. To make experimental investigation more efficient and economical, non-destructive, online monitoring of the crack development is employed. This work focuses on crack detection by acoustic emission (AE) methods, including the measurement setup and the evaluation of the acquired AE signals, while addressing common challenges such as background noise and data handling.

Keywords. Fatigue cracks, non-destructive testing, acoustic emission, pressure peaks

1. INTRODUCTION

As hydraulic components continue to evolve toward higher power densities and efficiencies, their structural design must meet increasingly demanding performance and reliability requirements. Achieving high power density often involves operating at elevated pressures or exploiting a weight-optimized design. Both require a targeted, sustainable use of material, particularly in highly stressed regions, which demands a precise understanding of the components' load limits.

A key failure mechanism is the initiation of fatigue cracks, which can have severe consequences, especially under cyclic internal pressure loading. Consequently, detailed knowledge of crack-growth behaviour is essential. Crack-propagation rates depend on the material properties and, above all, on the local stress amplitudes at the crack tip. [1] Furthermore, in oil environments, two opposing effects alter the stress amplitude compared with classical fracture-mechanics tests in air. On one hand, the crack faces are additionally loaded by the hydrostatic pressure of the oil, which increases the stress amplitude. Therefore, the crack propagates faster than without oil. However, there is an effect known as oil-

induced crack closure [2], which is illustrated in **Figure 1-1**. This effect is due to the viscous behaviour of the oil, which is particularly noticeable at high pressure drop rates. In this case, the oil cannot flow out of the crack sufficiently fast after the end of the load. The trapped oil prevents the crack faces from fully reclosing, sustaining residual internal pressure that lowers the effective stress amplitude (while the peak stress remains unchanged) and consequently extends component life. [3]

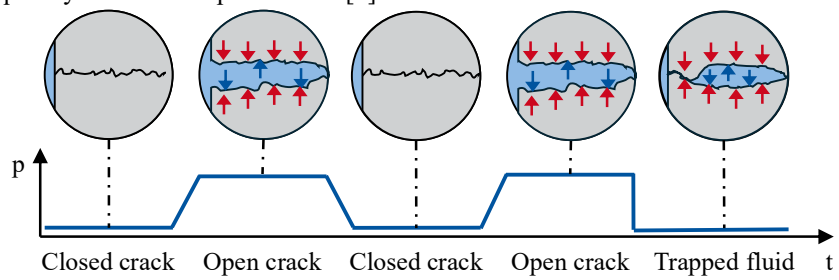

Figure 1-1: Oil-induced crack-closure caused by steep pressure drop rate.

Traditionally, hydraulic components are tested to failure under cyclic loading on pressure-impulse rigs, where cycle frequency significantly affects test duration and thus operating cost. Raising cycle frequency can substantially shorten operating time, in turn, steepen the load gradients, favouring oil-induced crack closure. Consequently, current testing relies on the incorrect assumption that component life is independent of cycle frequency, resulting in discrepancies between theoretical and experimental lifetime predictions [4].

To assess crack propagation during pressure-impulse testing, crack length must be evaluated at distinct intervals. Due to the large scope of the planned measurement series, manual measurement of the forcefully opened crack faces is not feasible. Therefore, this work develops a non-destructive, online monitoring method for hydraulic components to fundamentally investigate the influence of load frequency and pressure drop rates on crack propagation. For this purpose, samples are tested that are designed to initiate a well-defined crack quickly and sustain a steady propagation rate. The detection method involves using acoustic emission (AE) sensors, which are placed at suitable locations on the surface of the samples.

2. THEORY / STATE OF THE ART

The following sections provide the theoretical background and current state of research relevant to this work. They cover the fundamentals of fatigue crack growth, the influence of viscous fluids, and non-destructive testing techniques with a focus on acoustic emission methods.

2.1. Fatigue crack growth

Fatigue cracks are a critical failure mechanism in mechanical components, because they often develop unnoticed and do not cause a significant reduction in mechanical properties until critical failure. [5]

The process leading to final failure in metals, steels, and engineering alloys typically progresses through three distinct stages: nucleation, propagation, and breakthrough. Crack nucleation is the initial phase where microscopic damage begins to accumulate within the

material. This usually occurs under cyclic loading, even when the applied stress is below the material's yield strength. Localized plastic deformation occurs at microstructural imperfections due to dislocation activity, as the material seeks a lower energy configuration. In metals and alloys, persistent slip bands often form within grains and interact with grain boundaries, resulting in surface intrusions and extrusions that serve as early crack precursors. These imperfections can be intrinsic, such as inclusions, grain boundaries, or phase interfaces, or extrinsic, including surface defects like machining marks or scratches. Both types act as stress concentrators, accelerating local damage accumulation and promoting crack nucleation. Once nucleated, cracks begin to grow slowly and stably under continued loading, often referred to as the initiation phase. Initiation typically marks the onset of measurable crack growth from an initial micro-defect. [6]

To describe crack tip propagation, one must first address the mathematical singularity in the stress field at the crack tip [7]. Hence, the stress intensity factor (SIF) K is introduced to characterize this field in a finite and quantifiable manner, enabling calculation of crack growth by means of linear elastic fracture mechanics. It is dependent on the far-field applied stress σ, the current crack length a, and a geometric correction factor f, which accounts for geometry and orientation of the crack, with respect to the stress field. [1]

$$\Delta K = \Delta\sigma\sqrt{\pi a} \cdot f \tag{2-1}$$

Observing the change in SIF ΔK during cyclic loading of stress amplitude $\Delta\sigma$, one can describe the crack growth per cycle da/dN by the Paris-Erdogan equation [8]

$$\frac{\mathrm{da}}{\mathrm{dN}} = \mathrm{C} \cdot \Delta K^{m}, \tag{2-2}$$

with C and m being parameters determined by experimental material tests. The propagation phase can be divided into three phases, as can be seen in **Figure 2-1** in which the crack propagation rate per cycle is plotted against the change in SIF on logarithmic axes. Phase one characterizes the SIF region up to a threshold value ΔK_{th}. Up to this value, no crack propagation is expected. Phase two represents the stable crack growth region, characterized by a linear relationship between $log(da/dN)$ and $log(\Delta K)$, typically described by the Paris Law, extending up to the critical SIF range ΔK_c. Beyond this, in phase three, the crack grows rapidly and becomes unstable, leading to final fracture or breakthrough of the remaining cross-section. Thus, crack growth rate is influenced by the SIF range as well as the stress ratio R, which relates the maximum SIF to the minimum SIF. For a fixed ΔK, da/dN increases with R. Conversely, in the near-threshold regime, the threshold stress intensity factor ΔK_{th} decreases with increasing R [9].

The crack can propagate in relation to the direction of the applied far-field stress, as can be seen in Figure 2-1 on the right side, with three distinct modes identified: Mode I (opening mode), Mode II (sliding mode), and Mode III (tearing mode). In practical applications, a combination of these modes typically occurs. [10] However, this study specifically focuses on the effect of fluid on crack propagation under uniaxial loading of the crack faces subjected to normal stress, which corresponds exclusively to Mode I.

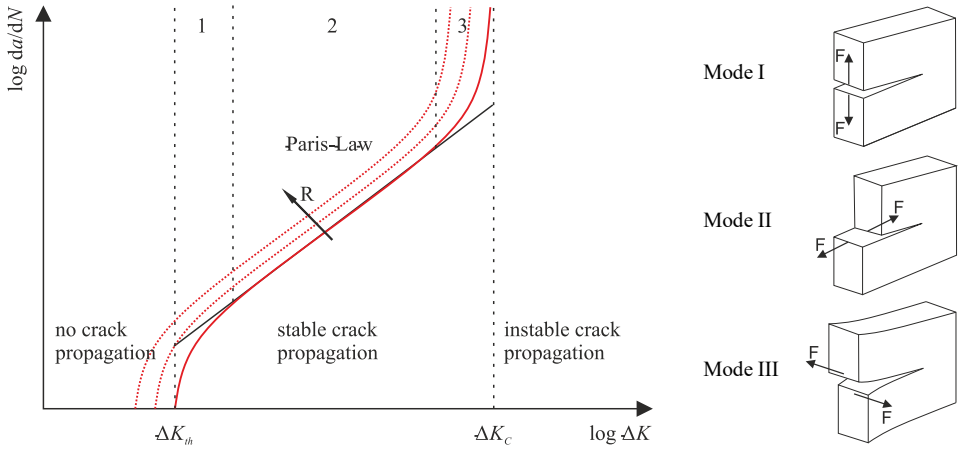

Figure 2-1: Crack growth rate with respect to the stress intensity range (left). Crack modes (right).

Little research has been conducted on the influence of fluid on the crack propagation, since typical metallurgical investigations are standardized and carried out in controlled environments [11]. In most tests, load is applied externally by special test rigs. However, these tests don't represent the real-world loading of cracked hydraulic components. Here, the load is applied directly on the crack faces as hydrostatic pressure. This is why most hydraulic components are subject to pressure impulse testing during development to determine load limits and lifetime.

Early research was conducted by Davis et al., who investigated the effect of oil under hydrostatic pressure on crack propagation in 1989. For this purpose, the specimen was subjected to cyclic mechanical loads in a pressure vessel. Depending on the type of loading, an improvement (tensile loading) or a deterioration (tensile-compressive alternating loading) of fatigue life was observed. [12]

In 2023, Michiels et al. examined both the influence of the pressure gradient [13] during cyclic pressure loading tests on crack growth and the effect of pulse frequency [14]. Additionally, they conducted and validated simulations to evaluate fluid behavior within a crack [3]. It was found that at very high pressure drop rates, oil can be trapped within the crack, as illustrated in Figure 1-1. This leads to a significant change in stress at the crack tip region, especially lowering the effective stress amplitude and thus extending fatigue lifetime. This phenomenon is known as oil-induced crack closure, where the presence of oil within the crack inhibits the crack faces from forming contact. A similar effect can occur due to roughness-induced crack closure, where surface irregularities cause early contact between crack faces, and oxide-induced crack closure, where oxidation products accumulate at the crack tip and impede full closure. [15]

To assess crack propagation rates, the crack length must be measured at defined intervals. In classical fatigue testing, cracks initiate and propagate along the surface and can be monitored using optical or mechanical methods, or through integrated measurement systems within the test rig. In contrast, cracks in hydraulic components, as well as in the specimens investigated in this study, form on the inner surfaces, making direct observation and

measurement significantly more challenging. Moreover, the pressure impulse test rig used in this work does not include built-in capabilities for crack length measurement. Consequently, non-destructive testing (NDT) methods must be employed.

The field of NDT for crack detection is vast, encompassing techniques based on electrical resistivity [16], ultrasonic energy [17], acoustic emission [18]–[21], and electromagnetic impedance [22], as well as digital image correlation [23]. Among these, the present work focuses on the application of AE testing, which enables the online and non-invasive detection of crack initiation and propagation processes during cyclic loading.

2.2. Acoustic emission testing

AE testing is a passive non-destructive testing technique utilized for monitoring the integrity and performance of solid materials, components and structures under stress. This method is based on the detection of high-frequency sound waves generated by the rapid release of energy from localized sources within a material, such as crack propagation, fiber breakage, or other forms of deformation. As these events occur, they emit elastic waves that can be captured by sensitive acoustic sensors such as piezoelectric sensors. In contrast to ultrasonic testing, which requires the active introduction of external acoustic energy, AE testing is considered passive, as it records signals that are naturally emitted by the material itself during loading. The sensors utilize a piezoelectric material that generates an electrical charge in response to mechanical stress. Sensor coupling to the specimen, as well as the setup of the amplification, filtering, and digitalizing devices, is essential for obtaining high quality signals with minimal influence of background noise. The schematics of AE sensor placement on the specimen and the acquired signal are shown in **Figure 2-2**. [24, 25]

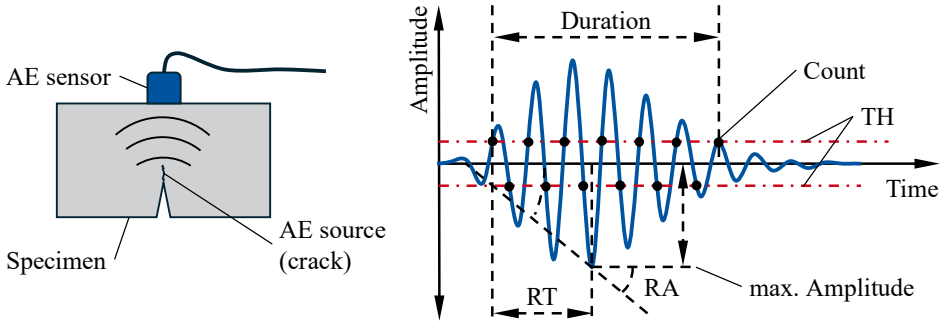

Figure 2-2: Illustration of AE sensor placement on specimen and AE source (left). Schematic AE signal amplitude over time (right) with signal parameters: Risetime (RT), riseangle (RA), duration, maximum amplitude, count of threshold (TH) crossing.

AE signals can be divided into continuous signals (e.g., process-related noise) and transient signals (signals with a recognizable beginning and end), often referred to as bursts [24]. While burst signals can be used to detect specific events such as crack growth, evaluation of continues signals at different time intervals allows for assessing structural changes or degradation over time. In fatigue and material testing burst signals are of primary importance. The raw signal is evaluated in the time and frequency domains to assess the presence of a burst and the corresponding crack propagation event [24]. **Figure 2-3** lists common signal processing approaches in the time domain. The raw signal (top) was created by a pencil lead break on the surface of an aluminium specimen.

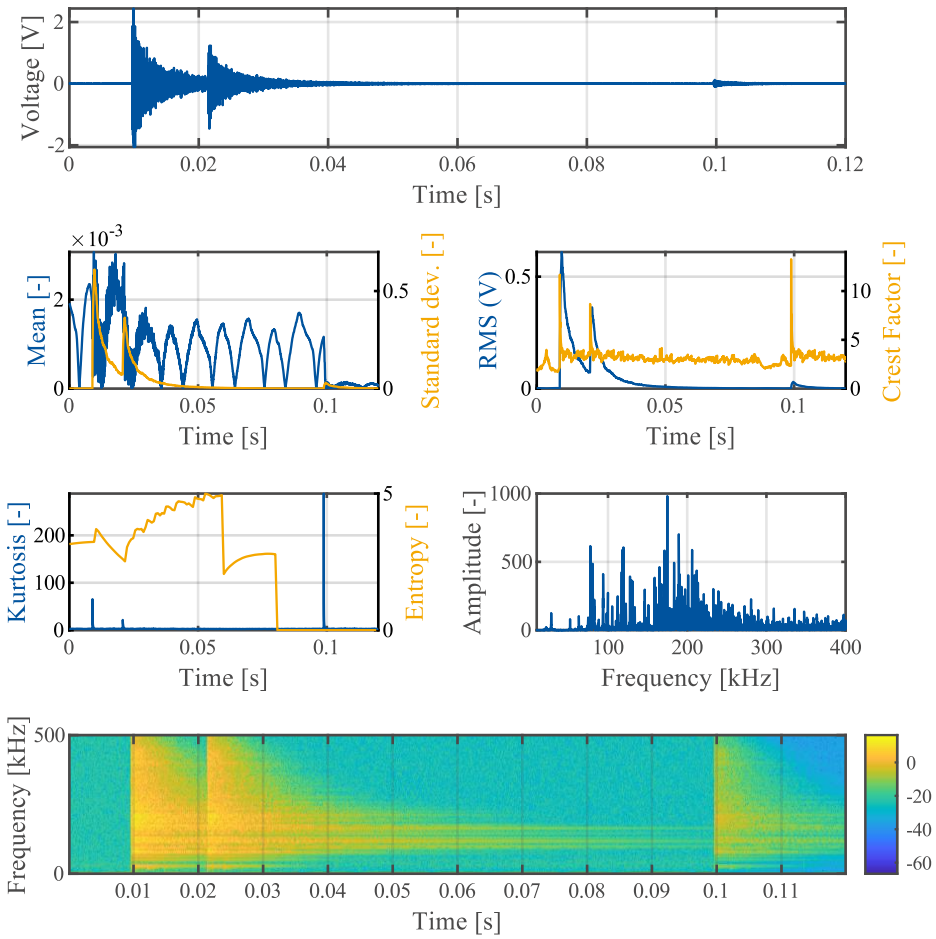

Figure 2-3: Time and frequency domain evaluation of raw signal (top).

Due to the axial symmetry of AE signals, the arithmetic mean often approaches zero, limiting its usefulness for analysis but forming the basis for further calculation. The root mean square (RMS) is the square root of the time-averaged squared measurements, allowing for burst signal evaluation and serving as a measure of signal energy. Variance and standard deviation indicate the dispersion of measurements relative to the mean, providing insights into burst presence: low variance suggests no bursts, while higher variance indicates their occurrence. The crest factor describes the ratio of peak value to RMS, with high values indicating isolated peaks with low energy. Finally, kurtosis measures the deviation from a Gaussian distribution; it equals 3 for normally distributed data and increases in the presence of bursts. In addition to analyzing time-domain parameters, AE signals can also be examined in the frequency domain. Two relevant methods for this study are the Fast Fourier Transform (FFT) and Short-Time Fourier Transform (STFT).

The presented time-domain approaches yield scalar values for a given signal. By applying windowing techniques, it becomes possible to track the temporal evolution of these signal properties, as summarized in Table 1. In the corresponding figures, the response of these

properties to transient signal components, such as bursts, can be clearly observed. Utilizing these processed signals together with appropriately defined threshold values, individual bursts can be detected and characterized. The resulting burst counts and their characteristic parameters can then be employed to evaluate the relationship between AE activity and the propagation of fatigue cracks.

3. METHOD

In the following, the test design, focussing on cyclic hydraulic loading, specimen design, and measurement strategy, is presented.

3.1. Test Design

The experiments are conducted on a pressure impulse test rig from Maximator [26], featuring a hydraulic power of 120 kW and maximum pressures of 1200 bar. This test rig generates a trapezoidal pressure profile with a frequency of 3 Hz, an upper pressure level of 400 bar, and a lower pressure level of 20 bar. The pressure increases at a rate of 20 kbar/s and decreases at 40 kbar/s. HLP46 serves as the pressure medium. **Figure 3-1** illustrates both the specified pressure cycle and the actual pressure during the cycle.

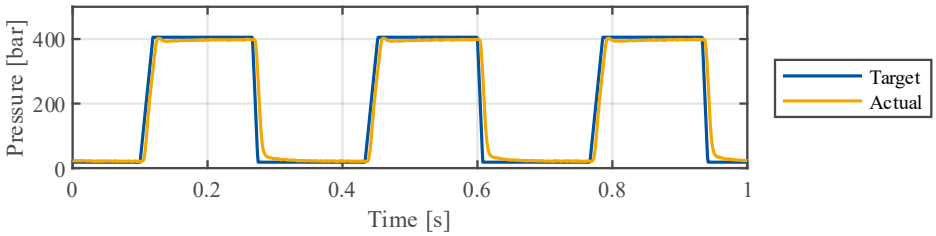

Figure 3-1: Target and actual pressure cycle at 3 Hz.

The geometry of the specimen made from steel S235 JR and the connection to the distribution manifold of the pressure impulse test rig is shown in **Figure 3-2**. The cavity inside the specimen is cyclically subjected to pressure during the experiment. At the base of the cavity, three holes are machined (see detail B) to facilitate fast crack formation due to local stress concentration. These specimens are designed to allow for stable crack growth under uniaxial hydraulic loading of the crack faces. Furthermore, a bleed plug is installed to allow for gas evacuation of the specimen. Bleeding is performed prior to each test run. Sealing the interface between the specimen and adapter is provided by a rubber O-ring.

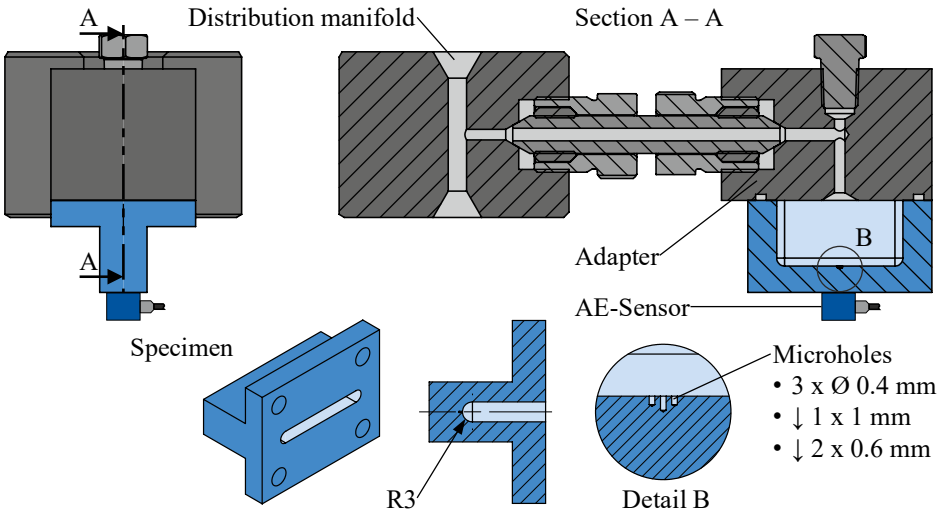

Figure 3-2: Specimen design and connection to pressure impulse test rig. Crack formation and growth is suspected to occur in section A-A of the specimen.

3.2. AE - Measurement setup

The AE sensor is mounted on the end face of the specimen using a magnetic holder, with wax serving as the coupling medium. A second AE sensor is placed at the corresponding position on a specimen without internal holes inside the cavity, hereafter referred to as the dummy specimen. Pressure sensors are installed at the distribution manifold, which are used to monitor and control the pressure profile (see **Figure 3-3).** During the experiment, signals from both AE sensors and a pressure sensor are recorded to evaluate AE activity in relation to the pressure cycle. To ensure temporal synchronization of the results, the signals are digitized using the same A/D converter. Piezotron® AE sensor type 8152C0 from Kistler is utilized. This sensor features an integrated preamplifier and has a sensitivity of 57 dB (ref. 1V) in the frequency range of 50 to 400 kHz. To amplify the AE signals further, Piezotron coupler type 5125C from Kistler is employed, which includes a tenfold amplification along with a 50 kHz high-pass filter and a 1000 kHz low-pass filter. The signals are digitized by the PCIe-6374 analog/digital converter from National Instruments at a maximum sampling rate of 3.5 MHz before being transmitted to the measurement computer. Both data acquisition and analysis are performed using MATLAB R2023b [27].

The high sampling rates required for the reliable detection of AE events result in a significant demand for storage space to capture the measurement data. One AE signal digitized at 3.5 MS/s with a sample size of 16 bits generates approximately 25 GB of measurement data per hour. Depending on the chosen loading frequency, test durations of several hours are expected. These large data volumes pose a challenge for continuous data acquisition, as the memory of the measurement computer will quickly become saturated. A similar issue also affects the evaluation process, as MATLAB requires all necessary variables and data to be present in memory. To address this, the data acquisition concept involves writing data in blocks of fixed sample size from memory to disk. A separate file is created for each block, and these files are numbered in the order of their creation. Specifically, data is acquired every 1000 load cycles over a period of 1 minute. Each acquisition sequence is further

divided into six consecutive blocks of 10 seconds each. This results in a large number of files, each containing a manageable amount of data, and prevents memory overflow during measurements, allowing for gradual evaluation of the measurement data. Figure 3-3 schematically illustrates the implemented data acquisition strategy, showing the periodic measurement intervals and the subdivision into time segments, as well as the sensor and specimen placement in the test chamber.

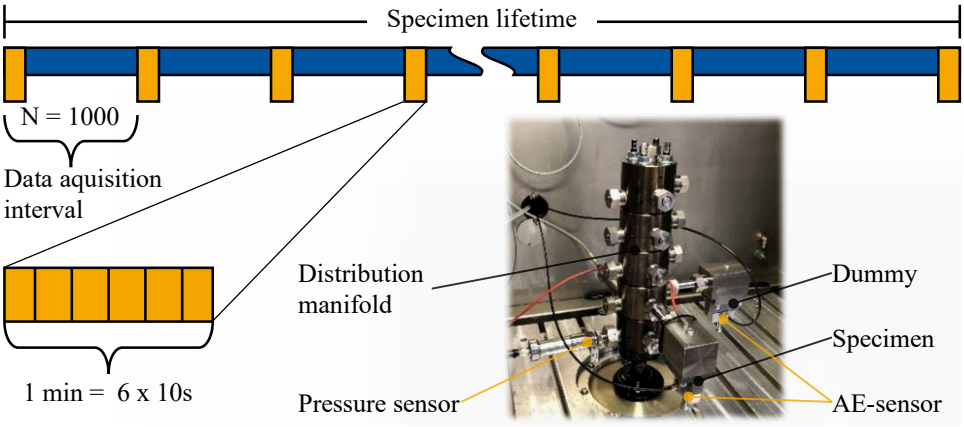

Figure 3-3: Schematic data acquisition strategy showing the periodic measurement intervals and the arrangement of sensors and specimens within the test chamber.

4. RESULTS

Final crack breakthrough of the investigated specimen occurred after 555.427 load cycles. AE and pressure data were acquired at intervals of 1000 cycles for both the test specimen and the dummy specimen, as shown in Figure 3-3. In the following, the raw AE signals of both specimens are presented for selected successive cycle numbers throughout the specimens' lifetime. Subsequently, AE bursts from both specimens are evaluated and characterized according to the methods described above. Finally, the bursts are analyzed in conjunction with the corresponding pressure signals.

Figure 4-1 shows AE signals of both specimens at the beginning of the test (N = 1k) as well as at intermediate cycle numbers in intervals of 100k cycles starting at N = 100k for the duration of 3 s or 10 load cycles, respectively. AE activity can be observed for the dummy specimen from the beginning of the test up to 500k cycles, exhibiting periodic bursts (3 Hz) with amplitudes of approximately ±0.011 V compared to a background noise level of ±0.003 V. This corresponds to a signal-to-noise ratio (SNR) of 3.7, which remains nearly constant throughout the test duration.

In contrast, the AE signal of the investigated specimen shows distinctly different behavior. No notable AE activity is detected during the initial 1000 cycles up to 300k cycles. A slight increase in amplitude is observed at 400k cycles (signal ±0.008 V, noise ±0.003 V, SNR = 2.7). At 500k cycles, the AE bursts become clearly distinguishable from the background noise, reaching amplitudes of around ±0.023 V (SNR = 7.7), indicating the onset of significant crack growth activity.

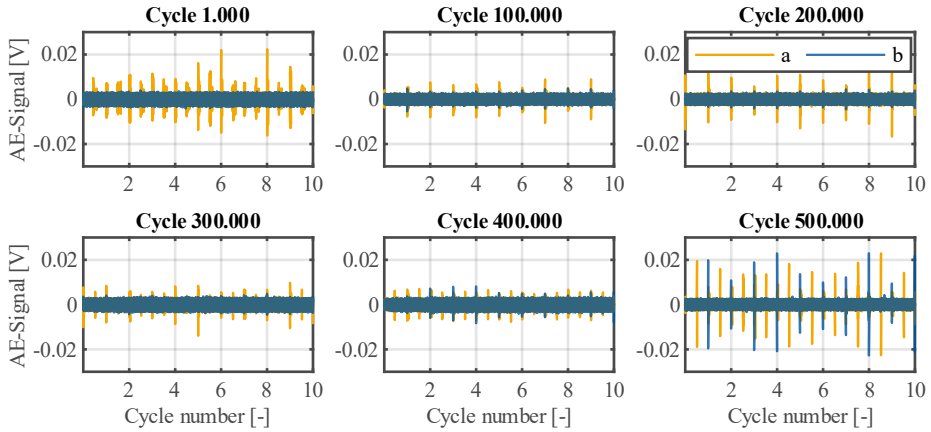

Figure 4-1: Raw AE signals at succeeding cycles for dummy (a) and specimen(b).

The increase in AE activity of the specimen between 400k and 500k cycles necessitates a more detailed examination of the period leading up to the end of the specimen's lifetime. Therefore, **Figure 4-2** focuses on the AE signals for selected cycle numbers closer to the specimen's final failure, shown in comparison with the dummy specimen.

At N = 545k, the specimen exhibits AE burst amplitudes ranging from approximately ±0.015 V to a maximum of ±0.030 V, with a background noise level of ±0.003 V, corresponding to a maximum SNR of 10. In the same interval, the dummy specimen shows a comparable maximum amplitude of ±0.021 V at similar noise levels.

At N = 550k, the specimen signal increases further, with amplitudes between ±0.018 V and ±0.037 V (SNR ≈ 12). The dummy specimen, however, shows only a single pronounced peak of about ±0.040 V, while the remaining signal remains around ±0.011 V with comparable noise (±0.003 V).

Shortly before final failure (N = 555k), the specimen signal exhibits a pronounced increase in AE activity, reaching amplitudes between ±0.050 V and up to ±0.140 V, resulting in a maximum SNR of 47. In contrast to previous intervals, the AE bursts no longer occur strictly at the load-cycle frequency. Instead, alternating high and lower peaks appear, effectively doubling the apparent signal frequency. The lower peaks reach amplitudes of approximately ±0.010 V (SNR ≈ 3). The dummy specimen signal remains largely unchanged during this stage.

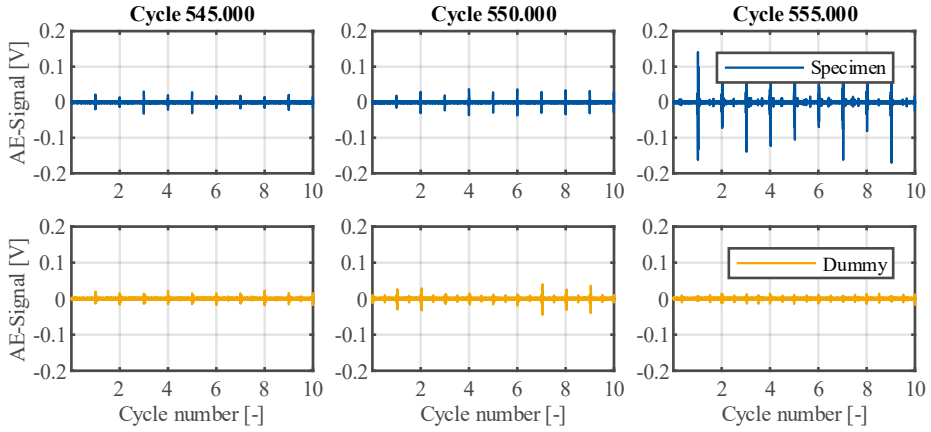

Figure 4-2: Raw AE signals at final succeeding cycles for both specimens.

As those results show distinct cases and a manual evaluation of the bursts of the time signals is not feasible, the method described above is applied to detect and characterize bursts. **Figure 4-3** presents the detected bursts of the specimen over the total test duration, obtained using different detection approaches. The methods include a static threshold applied to the raw signal, burst detection based on calculations in the time and frequency domains, and an entropy-based detection approach. From the bursts detected by those methods, mean values are calculated and compared with those of the dummy specimen, which were determined accordingly. The different detection methods exhibit varying sensitivities. When ranked by their overall sensitivity throughout the test, the methods can be ordered as follows: time-domain analysis (most sensitive), frequency-domain analysis, entropy-based detection, and finally, static thresholding.

The qualitative evolution of the detected burst rate shows no burst activity up to approximately 50k cycles, which aligns with the observations from the raw AE signals. From 50k to 300k, the detection rate remains nearly constant, with an average of around 100 bursts per minute. Between 300k and 400k cycles, a slight increase in detected bursts can be observed, followed by a more pronounced rise between 430k cycles and the end of the test, where all methods yield very similar burst rates of roughly 200 bursts per minute. Shortly before the final fracture, all methods indicate a sharp increase in AE activity. In contrast, the dummy specimen shows almost no detected bursts throughout the entire duration of the test, apart from a few sporadic detections.

It should be noted that data are missing for approximately 5k cycles at 100k, 200k, 300k, 400k, and 500k cycles. During these interruptions, the pressure profile was adjusted by changing the stress ratio from R = 0.05 to 0.6 at a maximum pressure of 400 bar. These steps were necessary to introduce optical beach marks on the fracture surface, allowing the crack growth path to be visually correlated with the corresponding cycle counts. After each change in stress ratio, the test system was restarted. In nearly all cases, a gradual increase in the number of detected bursts was observed immediately following each restart.

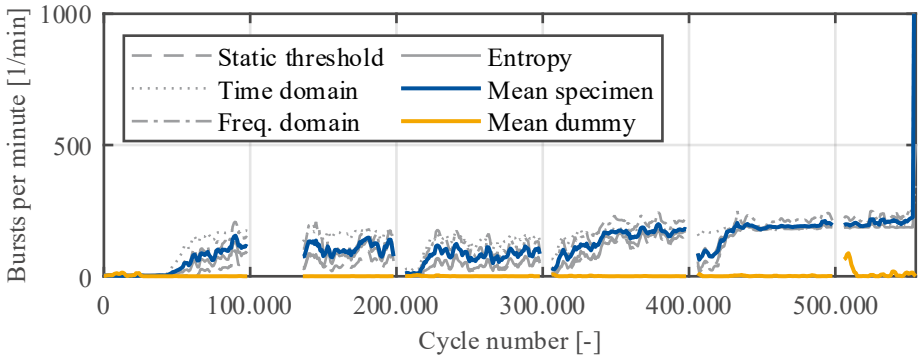

Figure 4-3: Results of burst detection with different approaches for both specimens.

Next, the focus is placed on the characterization of the detected bursts. For each identified burst, its amplitude, duration, and the number of threshold crossings are determined. During each acquisition phase (every 1k cycles for a period of 60 seconds), these parameters are averaged to obtain representative values. The normalized results are presented in **Figure 4-4** for the investigated and the dummy specimen.

The few bursts detected for the dummy specimen do not exhibit any consistent pattern or correlation, and there is almost no variation in their characteristic features from the beginning to the end of the test. In contrast, the burst features of the investigated specimen show a distinct evolution over time. The maximum values for amplitude, duration, and threshold crossings are observed near the end of the test, close to the point of final crack breakthrough. Similar to the trend in the overall burst count, these features remain nearly constant up to approximately 300k cycles, after which a gradual increase is observed, culminating in a pronounced rise shortly before failure.

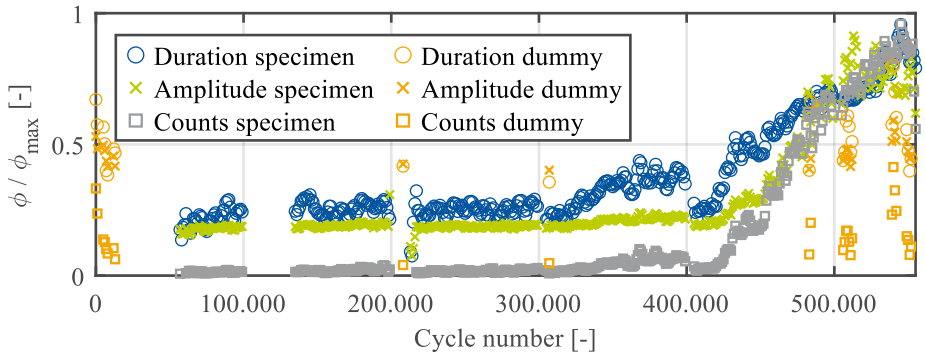

Figure 4-4: Characteristic features of detected bursts for both specimens.

To get a better understanding of the burst activity in relation to the load cycle, **Figure 4-5** illustrates the timing of cumulative burst occurrences within defined cycle intervals over one averaged pressure cycle. During the first 500k cycles, almost all bursts appear right at the onset of pressure increase (approximately 5.5 % of the cycle). As shown for the intervals between 510k to 550k cycles, both the timing of the bursts relative to the pressure rise and their count remain largely unchanged. Only during the last 5k cycles bursts also appear throughout the high-pressure phase.

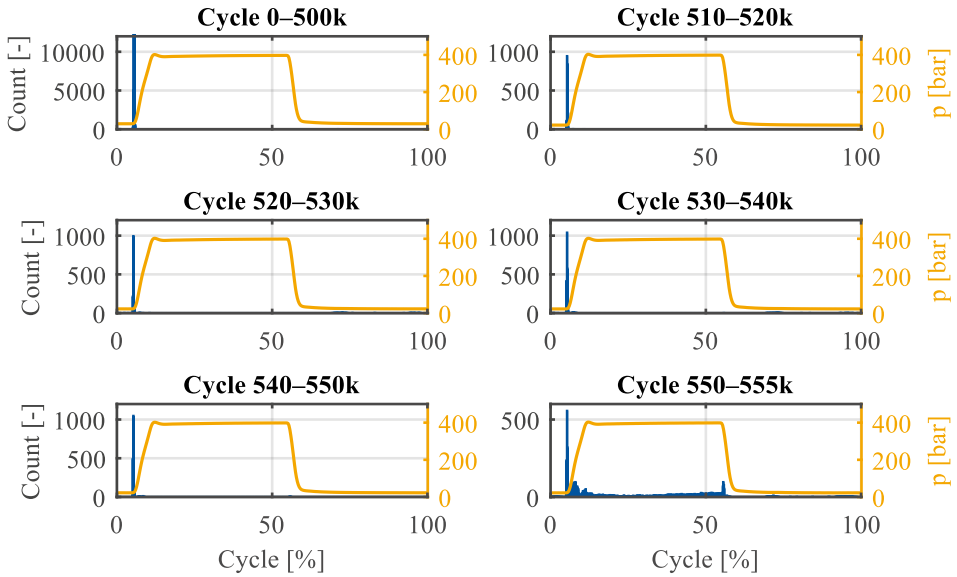

Figure 4-5: Cumulative cycle count for distinct intervals over pressure cycle.

5. DISCUSSION

The observed AE activity correlates strongly with the occurrence of cracking in the investigated specimen. Since the dummy specimen shows no notable change in signal characteristics, the AE sources in the specimen are likely associated with crack propagation. During the crack initiation phase, almost no AE activity is detected. This is followed by a long period of stable crack growth, characterized by nearly constant burst counts and signal features. Toward the end of the test, a phase of unstable crack growth is observed, during which both the number of detected bursts and their characteristic features (amplitude and duration) increase significantly.

However, it is unlikely that all AE activity originates solely from crack propagation. Other potential AE sources include plastic deformation, erosion, corrosion, impacts, and leakage. In addition, the pressure transducer and other hydraulic components in the pressure impulse test rig can generate spurious signals that interfere with AE detection and are audible to the human ear.

Interestingly, the highest AE activity is observed at the beginning of the pressure increase, when the maximum stress intensity at the crack tip has not yet been reached. This suggests that these detections are not only related to crack growth. Instead, they are likely associated with the sealing system of the specimen. The test specimen is sealed using an O-ring, which, due to design, exhibits slight play within its groove. Post-test inspection revealed some abrasion of the O-ring, indicating movement and potential gap extrusion, which could generate AE signals.

To mitigate this effect, a revised sealing concept is proposed, for example, using copper or flat gaskets to achieve a more stable and rigid seal. Additionally, flange deformation was observed during testing, which likely reduced the preload of the sealing assembly and further

contributed to AE noise. Future test setups will employ a stiffer specimen geometry and more uniform clamping with six instead of four bolts. These measures aim to minimize external interferences and enhance the reliability of AE-based crack detection.

To unambiguously attribute AE activity to the source of crack propagation, the implementation of a source localization strategy is suitable. By mounting two AE sensors on the same specimen, the origin of AE events can be determined from the arrival time difference of the signals in combination with the known acoustic wave velocity of the material [24].

To further improve signal quality, a noise-canceling approach can be implemented by using one AE sensor on the specimen and a second on the dummy specimen. The signal from the dummy specimen serves as a reference for background and system noise and can be subtracted from the specimen signal, for example, by applying methods such as continuous wavelet transform (CWT) or cross-correlation. This approach allows for the suppression of noise originating from the test setup, hydraulic system, or other external sources.

For signal evaluation, a manual analysis approach quickly becomes impractical due to the large volume of acquired data. Therefore, machine learning techniques are particularly suitable for the classification and analysis of AE signals. With the existing feature extraction (amplitude, duration, counts, entropy, etc.), the fundamental basis for applying such algorithms is already established. Future work may thus focus on developing automated workflows that use these features for clustering, pattern recognition, or predictive modeling of crack propagation behavior.

6. SUMMARY

This work demonstrates the application of AE techniques for the detection of fatigue cracks in hydraulic components during cyclic pressure impulse testing to investigate the influence of viscous fluids on crack propagation. The study introduces the experimental setup for both pressure impulse and AE measurements and addresses common challenges associated with AE measurements, such as the influence of background noise and the handling of large data volumes.

A dedicated data acquisition and evaluation framework was developed to capture and subsequently analyze AE signals during pressure impulse testing. The result shows crack propagation until final fracture. By comparing AE signals from the test specimen with those from a dummy specimen, which did not form cracks, AE activity related to crack growth could be identified.

Nevertheless, some uncertainty remains regarding the unambiguous attribution of AE activity to the crack propagation source, as AE signals are strongly affected by operational conditions, environmental influences, and especially sealing system behavior. Future work will focus on minimizing these uncertainties through optimized specimen and sealing design, as well as by advancing data analysis techniques using machine learning for automated signal classification and source localization.

ACKNOWLEDGMENTS

This work was funded by the German Research Foundation (DFG) in the scope of the Project „Einfluss der Belastungsgradienten auf das Ermüdungsverhalten hydraulischer Komponenten“ (449676223). The authors would like to thank DFG for its support.

7. REFERENCES

[1] Paris, P., Gomez, M., Anderson, W. ‘A rational analytic theory of fatigue’, The Trend in Engineering, pp. 9–14, 1961.

[2] Tzou, J.-L., Hsueh, C. H. et al. ‘Fatigue crack propagation in oil environments— II. A model for crack closure induced by viscous fluids’, Acta Metallurgica, Vol. 33, Nr. 1, pp. 117–127, 1985. DOI: 10.1016/0001-6160(85)90225-1.

[3] Michiels, L. ‘A simulation-based approach to the fluid-structure interaction inside fatigue cracks in hydraulic components’, Dissertation, Karlsruhe, 2024. DOI: 10.5445/IR/1000171515.

[4] Michiels, L., Geimer, M. ‘On the frequency dependency of fatigue damage caused by viscous fluid-structure interaction in hydraulic components’, Proceedings of the 18th Scandinavian International Conference on Fluid Power, 2023. DOI: 10.5445/IR/1000160350.

[5] Suresh, S. ‘Fatigue of materials’, 2. ed., reprint, Cambridge Univ. Pr, Cambridge, 2004. DOI: 10.1017/CBO9780511806575.

[6] Sangid, M. D. ‘The physics of fatigue crack initiation’, International Journal of Fatigue, Vol. 57, pp. 58–72, 2013. DOI: 10.1016/j.ijfatigue.2012.10.009.

[7] Sangid, M. D. ‘The physics of fatigue crack propagation’, International Journal of Fatigue, Vol. 197, pp. 108928, 2025. DOI: 10.1016/j.ijfatigue.2025.108928.

[8] Paris, P., Erdogan, F. ‘A Critical Analysis of Crack Propagation Laws’, Journal of Basic Engineering, Vol. 85, Nr. 4, pp. 528–533, 1963. DOI: 10.1115/1.3656900.

[9] Forman, R. G., Mettu, S. R. ‘Behavior of surface and corner cracks subjected to tensile and bending loads in Ti-6Al-4V alloy’, National Aeronautics and Space Administration, Houston, TX (USA). Lyndon B. Johnson Space Center, https://www.osti.gov/biblio/5555321, 1990.

[10] Irwin, G. R. ‘Analysis of Stresses and Strains Near the End of a Crack Traversing a Plate’, Journal of Appl. Mech., Vol. 24, Nr. 3, pp. 361–364, 1957. DOI: 10.1115/1.4011547.

[11] ASTM International: ‘ASTM E647-24 - Standard Test Method for Measurement of Fatigue Crack Growth Rates’, ASTM International, West Conshohocken, PA, 2024.

[12] Davis, F. H., Ellison, E. G., Plumbridge, W. J. ‘Effects of Hydrostatic Pressure on the Rate of Fatigue Crack Growth’, Fatigue & fracture of engineering materials & structures, Vol. 12, Nr. 6, pp. 511–525, 1989. DOI: 10.1111/j.1460-2695.1989.tb00560.x.

[13] Michiels, L., Geimer, M. ‘Influence of High Pressure Drop Rates on Fatigue Crack Growth’, Chemical Engineering & Technology, Vol. 46, Nr. 1, pp. 45–52, 2023. DOI: 10.1002/ceat.202200385.

[14] Michiels, L., Geimer, M. ‘Non-Destructive Pressure Pulse Examination for Fatigue Crack Detection in Hydraulic Components’, Proceedings of the ASME/BATH 2023 Symposium on Fluid Power and Motion Control, Sarasota, 16th-18th October 2023, 2023. DOI: 10.1115/FPMC2023-110728.

[15] Pippan, R., Hohenwarter, A. ‘Fatigue crack closure: a review of the physical phenomena’, Fatigue & fracture of engineering materials & structures, Vol. 40, Nr. 4, pp. 471–495, 2017. DOI: 10.1111/ffe.12578.

[16] Ritchie, R. O., Garrett, G. G., Knott, J. P. ‘Crack-growth monitoring: Optimisation of the electrical potential technique using an analogue method’, International Journal of Fracture Mechanics, Vol. 7, Nr. 4, pp. 462, 1971. DOI: 10.1007/BF00189118.

[17] Papazian, J., Nardiello, J., Silberstein, R., Welsh, G., Grundy, D., Craven, C., Evans, L., Goldfine, N., Michaels, J., & Michaels, T. ‘Sensors for monitoring early stage fatigue cracking’, International Journal of Fatigue, Vol. 29, 9-11, pp. 1668–1680, 2007. DOI: 10.1016/j.ijfatigue.2007.01.023.

[18] Deschanel, S., Ben Rhouma, W., Weiss, J. ‘Acoustic emission multiplets as early warnings of fatigue failure in metallic materials’, Scientific reports, Vol. 7, Nr. 1, pp. 13680, 2017. DOI: 10.1038/s41598-017-13226-1.

[19] Chai, M., Hou, X. et al. ‘Identification and prediction of fatigue crack growth under different stress ratios using acoustic emission data’, International Journal of Fatigue, Vol. 160, pp. 106860, 2022. DOI: 10.1016/j.ijfatigue.2022.106860.

[20] La Selle, T. de, Réthoré, J. et al. ‘Signatures of fatigue crack growth from acoustic emission repeaters’, Engineering Fracture Mechanics, Vol. 309, pp. 110388, 2024. DOI: 10.1016/j.engfracmech.2024.110388.

[21] Cui, J., Qu, X. et al. ‘Multi-parameter acoustic emission analysis for fatigue crack evaluation in structural health monitoring’, Measurement, Vol. 256, pp. 118529, 2025. DOI: 10.1016/j.measurement.2025.118529.

[22] Zilberstein, V., Schlicker, D. et al. ‘MWM eddy current sensors for monitoring of crack initiation and growth during fatigue tests and in service’, International Journal of Fatigue, Vol. 23, pp. 477–485, 2001. DOI: 10.1016/S0142-1123(01)00154-2.

[23] Gehri, N., Mata-Falcón, J., Kaufmann, W. ‘Automated crack detection and measurement based on digital image correlation’, Construction and Building Materials, Vol. 256, pp. 119383, 2020. DOI: 10.1016/j.conbuildmat.2020.119383.

[24] Grosse, C. U., Ohtsu, M. et al. ‘Acoustic Emission Testing - Basics for Research – Appl. in Engineering’, Springer eBook Collection, 2nd ed. 2022, Springer Int. Publishing; Imprint Springer, Cham, 2022. DOI: 10.1007/978-3-030-67936-1.

[25] The Japanese Society for Non-Destructive: ‘Practical Acoustic Emission Testing’, Springer, Tokyo, 2016. DOI: 10.1007/978-4-431-55072-3.

[26] Maximator GmbH: ‘Maximator GmbH’, https://www.maximator.com, 2025.

[27] The MathWorks Inc. ‘MATLAB Version 23.2 R2023b’, Massachusetts, USA, 2023.

Biographies

Lukas Boden obtained his master's degree in mechanical engineering at RWTH Aachen University in 2023. Since then, he is working as a research assistant at the Institute for Fluid Power Drives and Systems (ifas), focussing on identifying the influence of viscous fluid on fatigue crack propagation in fluid power components.

Fabian Blatter studied mechanical engineering at the Karlsruhe Institute of Technology. He is currently working as a Research Associate at the Department of Mobile Machines at the Karlsruhe Institute of Technology. His research areas include simulation of fluid-structure-interaction and hydraulic applications.

Prof. Dr.-Ing. Marcus Geimer received the Diploma degree in mechanical engineering from the RWTH Aachen University, Germany, in 1990, and the Ph.D. degree from the Institute of Hydraulics and Pneumatics, today named the Institute for Fluid Power Drives and Systems, RWTH Aachen University. Since 2005, he has been a Full Professor and the Director of the Institute of Mobile Machines (Mobima), Karlsruhe Institute of Technology

(KIT), Germany. He started his industrial career in 1995 in the field of construction at the company Krupp Berco Bautechnik GmbH, Germany, where he was the Leader of the research group for hydraulic breakers. In 2000, he was with Bucher Hydraulics GmbH, Germany, where he led the construction and customer development for mobile hydraulics.

Prof. Katharina Schmitz studied mechanical and chemical engineering at RWTH Aachen University and Carnegie Mellon University, Pittsburgh (USA) and graduated 2015 as Dr.-Ing. at RWTH Aachen University. Since 2018, she is full professor at RWTH Aachen University and director of the Institute for Fluid Power Drives and Systems (ifas). In addition, she is Vice Dean of the Faculty for Mechanical Engineering at RWTH Aachen, a position she holds since 2020. Prof. Schmitz's awards and honors include several best paper awards and 2023 IMechE Joseph Bramah Medal award.